

Recent progress on two-dimensional ferroelectrics: Material systems and device applications

Zhiwei Fan(范芷薇), Jingyuan Qu(渠靖媛), Tao Wang(王涛), Yan Wen(温滟), Ziwen An(安子文), Qitao Jiang(姜琦涛), Wuhong Xue(薛武红), Peng Zhou(周鹏), and Xiaohong Xu(许小红)
Citation: Chin. Phys. B, 2023, 32 (**12**): 128508. DOI: 10.1088/1674-1056/ad08a4
Journal homepage: http://cpb.iphy.ac.cn; http://iopscience.iop.org/cpb

What follows is a list of articles you may be interested in

Ultra-high photoresponsive photodetector based on ReS_2/SnS_2 heterostructure

Binghui Wang(王冰辉), Yanhui Xing(邢艳辉), Shengyuan Dong(董晟园), Jiahao Li(李嘉豪), Jun Han(韩军), Huayao Tu(涂华垚), Ting Lei(雷挺), Wenxin He(贺雯馨), Baoshun Zhang(张宝顺), and Zhongming Zeng(曾中明)
Chin. Phys. B, 2023, 32 (**9**): 098504. DOI: 10.1088/1674-1056/acd9c0

Graphene-based heterojunction for enhanced photodetectors

Haiting Yao(姚海婷), Xin Guo(郭鑫), Aida Bao(鲍爱达), Haiyang Mao(毛海央),Youchun Ma(马游春), and Xuechao Li(李学超)
Chin. Phys. B, 2022, 31 (**3**): 038501. DOI: 10.1088/1674-1056/ac1b8b

A double quantum dot defined by top gates in a single crystalline InSb nanosheet

Yuanjie Chen(陈元杰), Shaoyun Huang(黄少云), Jingwei Mu(慕经纬), Dong Pan(潘东), Jianhua Zhao(赵建华), and Hong-Qi Xu(徐洪起)
Chin. Phys. B, 2021, 30 (**12**): 128501. DOI: 10.1088/1674-1056/abff2e

Effect of electrical contact on performance of WSe_2 field effect transistors

Yi-Di Pang(庞奕荻), En-Xiu Wu(武恩秀), Zhi-Hao Xu(徐志昊), Xiao-Dong Hu(胡晓东), Sen Wu(吴森), Lin-Yan Xu(徐临燕), and Jing Liu(刘晶)
Chin. Phys. B, 2021, 30 (**6**): 068501. DOI: 10.1088/1674-1056/abd752

Determining the influence of ferroelectric polarization on electrical characteristics in organic ferroelectric field-effect transistors

Fu Zong-Yuan (浮宗元), Zhang Jian-Chi (张剑驰), Hu Jing-Hang (胡静航), Jiang Yu-Long (蒋玉龙), Ding Shi-Jin (丁士进), Zhu Guo-Dong (朱国栋)
Chin. Phys. B, 2015, 24 (**5**): 058502. DOI: 10.1088/1674-1056/24/5/058502

TOPICAL REVIEW — Post-Moore era: Materials and device physics

Recent progress on two-dimensional ferroelectrics: Material systems and device applications

Zhiwei Fan(范芷薇)[1,†], Jingyuan Qu(渠靖媛)[1,†], Tao Wang(王涛)[1], Yan Wen(温滟)[1], Ziwen An(安子文)[1], Qitao Jiang(姜琦涛)[1], Wuhong Xue(薛武红)[1,‡], Peng Zhou(周鹏)[2,§], and Xiaohong Xu(许小红)[1,¶]

[1] *Key Laboratory of Magnetic Molecules and Magnetic Information Materials of Ministry of Education and School of Chemistry and Materials Science, Shanxi Normal University, Taiyuan* 030031, *China*

[2] *State Key Laboratory of ASIC & System, School of Microelectronics, Fudan University, Shanghai* 200433, *China*

(Received 31 July 2023; revised manuscript received 20 October 2023; accepted manuscript online 2 November 2023)

Ferroelectrics are a type of material with a polar structure and their polarization direction can be inverted reversibly by applying an electric field. They have attracted tremendous attention for their extensive applications in non-volatile memory, sensors and neuromorphic computing. However, conventional ferroelectric materials face insulating and interfacial issues in the commercialization process. In contrast, two-dimensional (2D) ferroelectric materials usually have excellent semiconductor performance, clean van der Waals interfaces and robust ferroelectric order in atom-thick layers, and hold greater promise for constructing multifunctional ferroelectric optoelectronic devices and nondestructive ultra-high-density memory. Recently, 2D ferroelectrics have obtained impressive breakthroughs, showing overwhelming superiority. Herein, firstly, the progress of experimental research on 2D ferroelectric materials is reviewed. Then, the preparation of 2D ferroelectric devices and their applications are discussed. Finally, the future development trend of 2D ferroelectrics is looked at.

Keywords: two-dimensional materials, ferroelectrics, device applications

PACS: 85.30.–z, 77.80.–e, 28.52.Fa **DOI:** 10.1088/1674-1056/ad08a4

1. Introduction

Ferroelectric materials are a class of functional materials with important properties such as piezoelectricity, ferroelectricity, pyroelectricity and the photoelectric effect. They are widely used in non-volatile memory, field-effect transistors, solar cells, sensors, photonic devices, etc. In 1921, Valasek reported the existence of 'permanent polarization in the natural state' and hysteresis effects in potassium sodium tartrate crystals, and this result marked the formal discovery of the ferroelectric phenomenon.[1] In 1933, Busch and Scherrer discovered that potassium dihydrogen phosphate exhibited ferroelectricity below 122 K.[2] However, technical application of potassium sodium tartrate and potassium dihydrogen phosphate was difficult to achieve. It was not until the 1950s that Wainer and Salomon first deposited ferroelectric thin films with a perovskite structure and discovered strong ferroelectricity at room temperature.[3] With the rapid development in miniaturization of electronic devices, there is a pressing need for miniaturized, densely integrated electronic devices. However, when a ferroelectric material is below a critical thickness, the stability of ferroelectric thin films decreases due to the intrinsic effect and depolarization field, which poses great challenges for the development of nanoelectronic devices based on traditional ferroelectric materials. Extensive efforts have been made by researchers to overcome these difficulties. Following the discovery of ferroelectricity in polyvinylidene fluoride[4] and its copolymer with trifluoroethylene (VDF-TrFE)[5] in the 1980s, ferroelectricity was observed in two-monolayer-thick copolymers of polyvinylidene fluoride and vinylidene trifluoride in 1998.[6] Later, in 2019, Ji *et al.*[7] reported that free-standing $BiFeO_3$ film as thin as two unit cells exhibited stable ferroelectricity. Piezoresponse force microscopy (PFM) measurements of the films showed clear hysteresis loops, demonstrating switchable polarization. This work breaks the size effect faced by conventional ferroelectric materials. In 2020, Cheema *et al.*[8] reported that ultrathin (1 nm) zirconium-doped hafnium oxide (HZO) with a fluorite structure had stable ferroelectricity. Compared with conventional chalcogenide ferroelectric materials, this report indicated that HZO tends to change from a paraelectric phase with low symmetry to a ferroelectric phase with high symmetry as the thickness decreases, which results in a vanishing critical thickness and enhanced spontaneous polarization. These properties are in contrast to the critical size effect exhibited by conventional ferroelectric materials. So far, conventional ferroelectric materials have been realized at the nanoscale; however, it should be noted that the preparation of high-quality ferroelectric films depends critically on substrate selection and the preparation

[†]These authors contributed equally to this work.
[‡]Corresponding author. E-mail: xuewuhong@sxnu.edu.cn
[§]Corresponding author. E-mail: pengzhou@fudan.edu.cn
[¶]Corresponding author. E-mail: xuxh@sxnu.edu.cn

© 2023 Chinese Physical Society and IOP Publishing Ltd

method, which places limitations on the widespread development of nanoelectronics.

Since the successful exfoliation of graphene in 2004,[9] the family of two-dimensional (2D) materials has continued to expand. 2D van der Waals (vdW) materials provide a platform for achieving ferroelectricity at the atomic scale due to their naturally stable layered structure, surface-saturated chemistry and weak interactions between layers. With the growing interest in 2D materials, thousands of 2D materials have been discovered, including transition metal dichalcogenides (TMDs),[10–13] hexagonal boron nitride (hBN)[14], MXenes,[15–17] Xenes,[18–23] organic materials,[24–28] etc. Currently, 2D ferroelectric materials have been demonstrated to have potential applications in ferroelectric tunnel junctions,[29,30] ferroelectric diodes,[31] negative capacitance transistors,[32] semiconductor field-effect transistors,[33] nanophotonic devices[34] and neurosynaptic devices.[35]

In recent years, many advances have been made in the study of 2D ferroelectric materials, both theoretically and experimentally. In this review, we first describe the development of some intrinsic and non-intrinsic 2D ferroelectric materials. Then, we summarize the specific applications of the current popular 2D ferroelectrics, such as ferroelectric semiconductor field-effect transistors, synaptic simulation, photovoltaic storage, etc. Finally, we provide an outlook on the challenges and opportunities in 2D ferroelectric material research.

2. Two-dimensional ferroelectric materials

2.1. The 2D semiconductor ferroelectric materials

2.1.1. $CuInP_2S_6$

$CuInP_2S_6$, a member of the transition metal thiophosphorus (TMTP) family, has attracted special attention due to its potential ferroelectricity. As shown in Fig. 1(a), the atomic structure of $CuInP_2S_6$ is a sulfur framework with the octahedral voids filled by Cu, In and P–P patterns. The exchange of sites between Cu and P–P pairs makes a complete unit cell composed of two single molecular layers. In 2015, Belianinov *et al.*[36] first reported that 50-nm-thick layered $CuInP_2S_6$ has out-of-plane (OOP) ferroelectricity, and when the temperature was reduced to the phase transition temperature T_c (315 K), due to the displacement of the Cu sublattice from a centrosymmetric position to the In sublattice, spontaneous polarization of the vertical layer planes occurred. Furthermore, by varying the atomic ratio between Cu and In, Susner *et al.*[37] fabricated 20-nm-thick $CuInP_2S_6$ flakes with enhanced ferroelectricity. Later, Liu *et al.*[30] reported room-temperature OOP ferroelectricity of $CuInP_2S_6$ flakes of different thicknesses achieved by mechanical exfoliation. Figures 1(b) and 1(c) represent the ferroelectric amplitude and phase diagrams of $CuInP_2S_6$ flakes of different thicknesses. According to that report, polarization reversal was observed in a 4 nm $CuInP_2S_6$ flake with a phase transition temperature of about 320 K. The opposing quasi-dipole within $CuInP_2S_6$ greatly reduces the depolarization field, enabling stability of polarization down to ultrathin thicknesses.

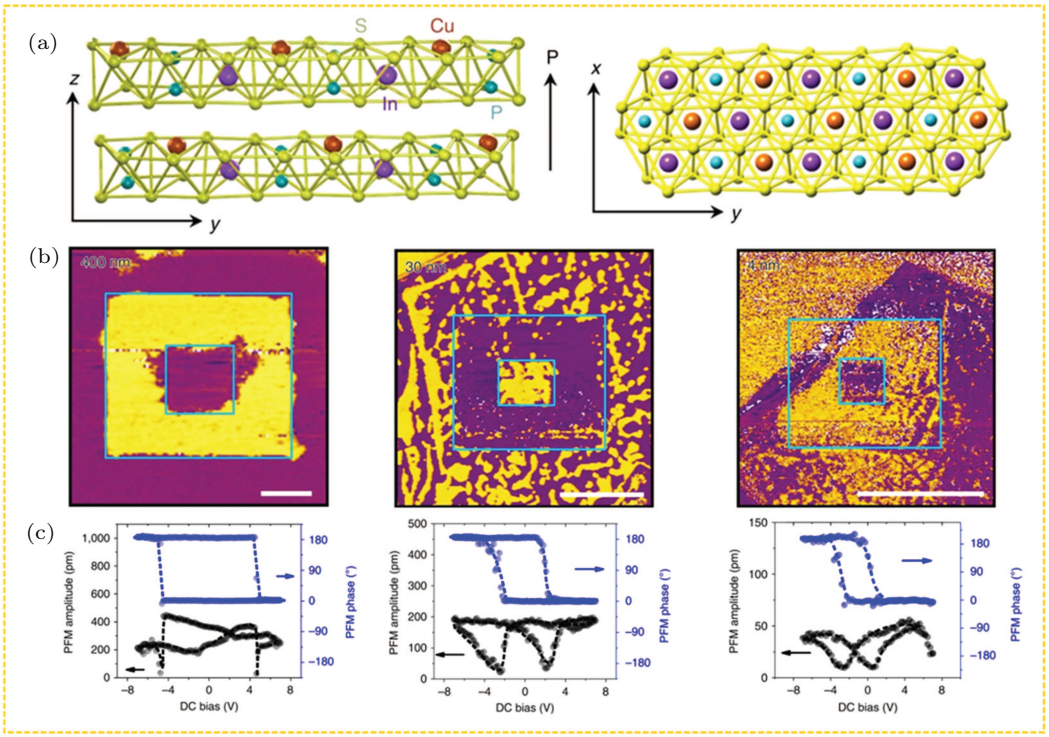


Fig. 1. (a) The crystal structure of $CuInP_2S_6$. (b) PFM phase images of $CuInP_2S_6$ flakes of different thicknesses, under reverse DC bias, written with a box-in-box pattern. (c) Corresponding PFM amplitude (black) and phase (blue) hysteresis loops for different thicknesses of $CuInP_2S_6$ flakes during the switching process. Reproduced with permission from Ref. [30].

2.1.2. In_2Se_3

In_2Se_3 is an n-type layered ferroelectric semiconductor. Monolayer In_2Se_3 consists of Se and In atoms with covalent bonding and it contains five atomic layers stacked in the sequence Se–In–Se–In–Se.[38] Its ferroelectricity was first predicted by structural analysis in 1990,[39] then it was theoretically predicted to have both in-plane (IP) and OOP ferroelectric polarization. In 2017, Ding *et al.*[40] calculated the structure of five-layer In_2Se_3 (Fig. 2(a)). It was predicted that In_2Se_3 presents both IP and OOP spontaneous polarization due to the movement of Se atoms breaking the central symmetry and has intercorrelated IP and OOP ferroelectricity originating from the electric field-induced lateral movement of the central Se atomic layer (Fig. 2(b)). In 2018, Cui *et al.*[41] prepared ultrathin nanoflakes of 2D layered α-In_2Se_3 and confirmed IP and OOP ferroelectricity at room temperature. They also found using PFM that the OOP polarization reversal also leads to a flip in IP polarization under a vertical electric field (Fig. 2(c)). A butterfly-like voltage-dependent amplitude loop and the change in phase up to 180° demonstrate OOP polarization switching (Fig. 2(d)).[42] In the same year, Xue *et al.*[43] also measured stable IP and OOP ferroelectricity of α-In_2Se_3 nanoflakes with different thicknesses at room temperature. The asymmetric structure was characterized using SHG and it was proposed that the ferroelectric polarization was due to the unequal spacing between the Se atomic layer and the two neighboring In atomic layers. In 2020, Io *et al.*[44] reported that the ferroelectric properties of 10-nm-thick α-In_2Se_3 can be maintained up to 200 °C. This result presents opportunities for new applications of 2D ferroelectric materials in high-temperature nanoelectronic devices. In 2021, Lv *et al.*[45] used physical vapor deposition technology to prepare ultra-large (up to 200 μm) α-In_2Se_3 nanoflakes, and found that 2H α-In_2Se_3 has layer-dependent ferroelectric polarization. The odd layer has a large IP polarization and is capable of polarization reversal due to the correlation between IP and OOP polarization; a similar layer-dependent OOP polarization occurs when the IP polarization is reversed by an electric field. In 2022, Lv *et al.*[46] reported muti-level memory of 2H α-In_2Se_3 by modulating the polar order with application of an in-plane electric field. The memory has a fast switching speed and excellent endurance and retention. It is worth noting that reversible switching between intermediate- and low-resistance states can be achieved by an ultra-low electric field that is one to two orders of magnitude smaller than that of other 2D ferroelectric materials; this is desired for low-power devices. In addition to In_2Se_3, InSe has also been reported to have synergistic ferroelectricity.[47,48]

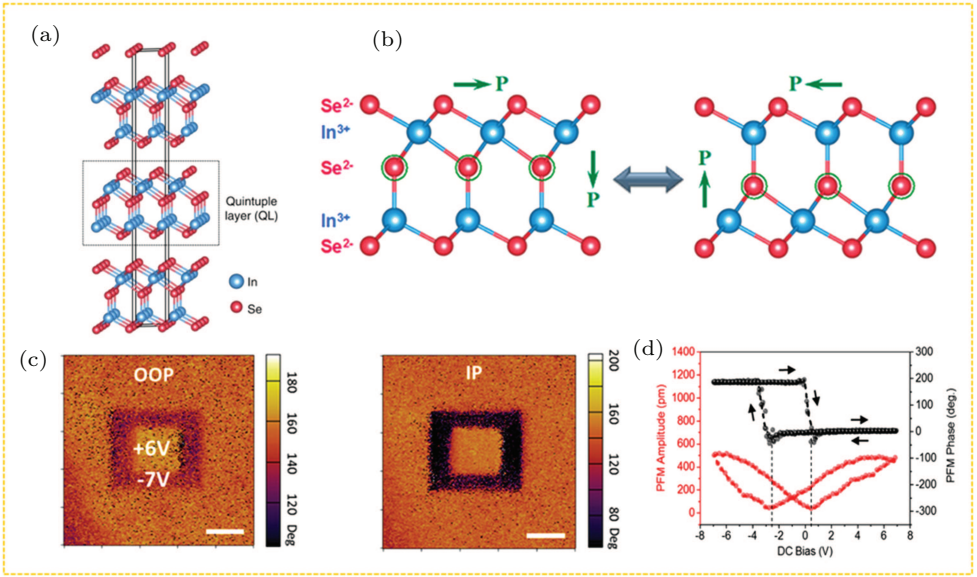


Fig. 2. (a) The crystal structure of layered In_2Se_3 with the In atoms in blue and Se atoms in red. A quintuple layer is indicated by the black dashed square. (b) Schematic model of IP and OOP polarization switching coupling. (c) OOP phase image and the corresponding IP phase image of a 6 nm thick In_2Se_3 flake acquired immediately after writing two square patterns with a size of 2 μm and 1 μm by applying voltages of −7 V and +6 V consecutively. The scale bar is 1 μm. (d) Local PFM hysteresis curves of In_2Se_3. Reproduced with permission from Refs. [40–42].

2.1.3. SnS

The fourth main group of materials, *MX* monosulfides (M = Ge, Sn; X = S, Se), has a large IP spontaneous polarization. In 2016, Wu and Zeng[49] predicted ferroelectricity in monolayer phosphorene analogues (SnS and SnSe) based on density functional theory (DFT) calculations. In 2020, Higashitarumizu *et al.*[50] reported that few-layer (fewer than 15 layers) tin sulfide (SnS) crystals have strong IP ferroelectricity; this was attributed to the different stacking order of the cross-sectional crystal structure along the armchair direction with the centrosymmetric AB stacking on the left and the non-centrosymmetric AA stacking on the right (Fig. 3(a)).

That work verified IP ferroelectricity by double-wave measurements on two-terminal SnS devices (Fig. 3(b)). Each measurement was performed by applying a voltage from 0 to 2 V twice, followed by the application of a voltage from 0 to −2 V twice (top panel of Fig. 3(c)). In the meantime, the current between the source and drain was recorded upon application of the voltage (bottom panel of Fig. 3(c)). It was found that a current peak was generated in the first scan but not in the second scan, because polarization switching occurs only in the first sweep and the direction of polarization does not change in the second sweep. Thus, the result of double-wave measurement unambiguously confirms IP ferroelectricity of SnS.

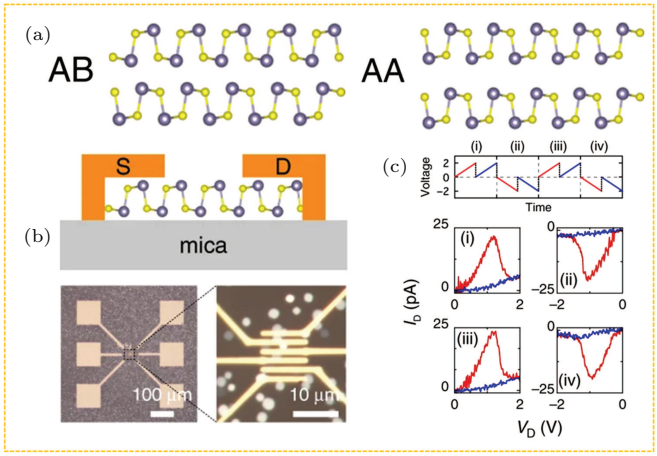


Fig. 3. (a) Cross-sectional crystal structures of SnS with different stacking sequences. (b) Cross-sectional schematic and optical images of two-terminal SnS devices. (c) Double-wave measurement. Reproduced with permission from Ref. [50].

IP ferroelectrics are superior to OOP and interlocked ferroelectrics in preventing depolarization fields.

2.2. The 2D (half-)metallic ferroelectric materials

2.2.1. WTe_2

Polar metals are very rare because itinerant electrons screen electrostatic forces between ions. But in 1965, Anderson and Blount predicted the possibility of a ferroelectric metal.[51] It was not until 2013 that the metallic material $LiOsO_3$ with a polar structure was experimentally verified by resistivity measurements and neutron diffraction. It was shown that at 140 K, the Li ions in $LiOsO_3$ moved along the extended [111] axis and the structure changes from centrosymmetric to non-centrosymmetric.[52] The discovery of polar metallic materials makes ferroelectric metals very attractive. The topological semimetal WTe_2 has been reported to have ferroelectricity.[53–55] In 2018, Fei *et al.*[53] demonstrated that when WTe_2 is thin enough its polarity can be reversed by applying an electric field. Although it is well known that monolayer WTe_2 is centrosymmetric and thus non-polar, the stacked bulk structure is polar. Therefore, multilayer WTe_2 can exhibit spontaneous electric polarization. Figure 4(a) shows the structure of three-dimensional 1T′-WTe_2: the polarization axis (*c*-axis) is parallel to both the *b*–*c* mirror (M) and *a*–*c* glide (G) planes. Applying an electric field to the polarization axis, as shown in the inset of Fig. 4(b), a bistability characteristic of the conductance was observed in trilayer

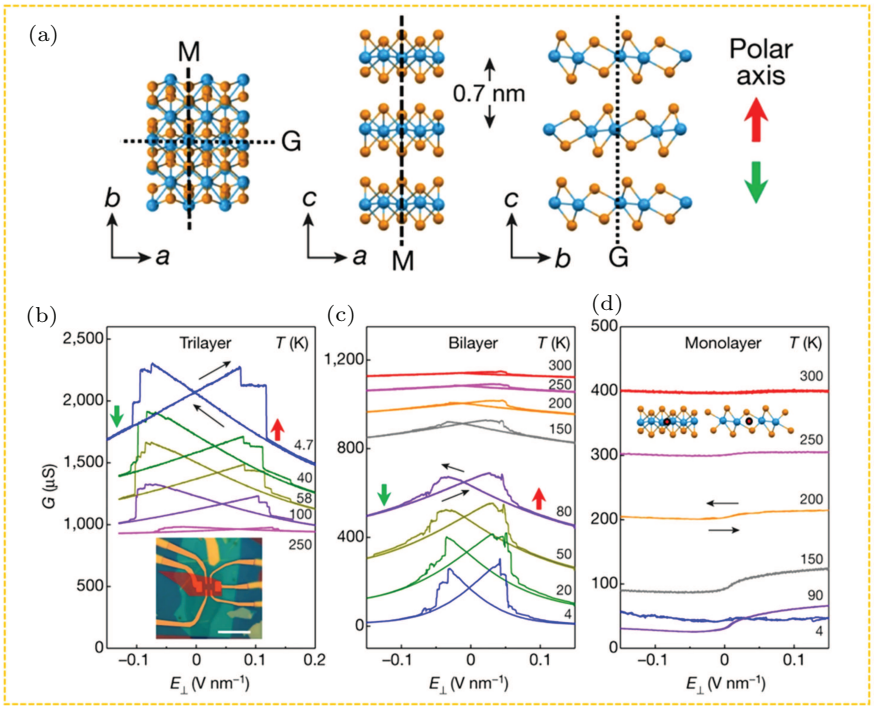


Fig. 4. (a) Structure of the three-dimensional 1T′-WTe_2. W atoms are blue and Te atoms are orange. (b)–(d) Conductance (G) of an undoped trilayer device (b), bilayer device (c) and monolayer device (d). Reproduced with permission from Ref. [53].

(Fig. 4(b)) and bilayer (Fig. 4(c)) devices, indicating ferroelectric switching. In contrast, there is no bistability in monolayer WTe_2 (Fig. 4(d)). These results also provide a hint that the spontaneous polarization in WTe_2 is driven by electron–hole correlation effects rather than lattice distortion.

2.2.2. Bimetal phosphates ($M_IM_{II}P_2X_6$)

The ferroelectricity of 2D bimetallic phosphates has been predicted to stem from spontaneous symmetry breaking caused by opposite displacements of bimetallic atoms, with full-d-orbital coinage metal elements causing larger displacements and polarizations than other elements.[55] For 2D ferroelectric metals, the odd number of electrons per cell without spin polarization may lead to a half-full energy band near the Fermi energy level and give rise to the metallicity. Results show that the conducting electrons move mainly on one side of the surface of the 2D layer, while both the ionic and electrical contributions to the polarization come from the other side and are perpendicular to the upper layer, leading to the coexistence of metallicity and ferroelectricity. Taking $AuZrP_2S_6$ and $InZrP_2Te_6$ as typical examples, they show non-centrosymmetry (Fig. 5(a)), where the corresponding polarization points in an OOP direction and the metal atoms with their larger displacements dominate the polarization. For each of $InZrP_2Te_6$ and $AuZrP_2S_6$ there is an energy band that crosses the Fermi energy level, indicating a metallic character (Figs. 5(b) and 5(c)). The chemical nature of the M_I sites causes them to deviate from their high-symmetry position and move to the lower surface (Figs. 5(d) and 5(e)), having a large movement and allowing the major ions to contribute to the polarization, indicating a ferroelectric character.

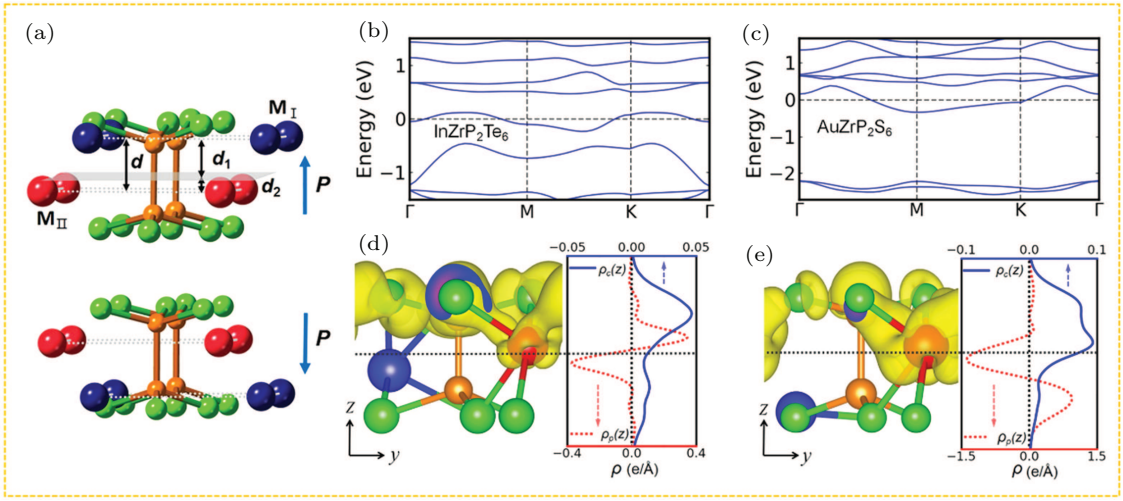


Fig. 5. (a) Side view of type I low-symmetry phases. (b), (c) Band structures of two ferroelectric metals: $InZrP_2Te_6$ and $AuZrP_2S_6$. (d), (e) Top and side views of partial electron density. Reproduced with permission from Ref. [55].

2.2.3. Distorted 1T-$MoTe_2$

Theoretical studies have provided insight into the ferroelectric origin of the d1T-AB_2 (A = Cr, Mo, W, and B = S, Se, Te) monolayer TMD system, and the Jahn–Teller effect and strong covalent bonding between transition metal atoms were believed to play key roles.[56,57] In 2019, Yuan *et al.*[58] found strong room-temperature OOP ferroelectricity in monolayer $MoTe_2$ with a distorted 1T (d1T) phase. The d1T phase was formed by laser processing of 2H $MoTe_2$ accompanied by the emergence of Te vacancies, which causes a few Te atoms to move towards the Mo plane in the OOP direction and generate spontaneous OOP polarization (Fig. 6(b)). The origin of ferroelectricity in d1T-$MoTe_2$ is due to spontaneous symmetry breaking caused by the relative atomic displacements of Mo and Te atoms. Based on the difference in charge density between the ferroelectric d1T and paraelectric 1T phases, the summed IP dipoles are determined to be zero (Figs. 6(a) and 6(d)). Therefore, a non-zero dipole is only present in the OOP direction (Fig. 6(e)), leading to stable ferroelectricity perpendicular to the lattice plane. Furthermore, the presence of switchable ferroelectric polarization in ultrathin samples was demonstrated using PFM. Figure 6(c) shows the phase and amplitude hysteresis loops of d1T-$MoTe_2$ at room temperature. The phase contrast between the two polarization states is 180° and the minimum value in the amplitude loop coincides with the switching voltage in the phase signal, indicating room-temperature ferroelectricity. Figure 6(f) further verifies its ferroelectricity by performing a PFM phase reversal test, where the electric poling was performed by writing two square patterns with ±8 V. The PFM phase contrast in the two square patterns reaches ∼ 180°, confirming anti-parallel electrical polarization in the two ferroelectric domains.

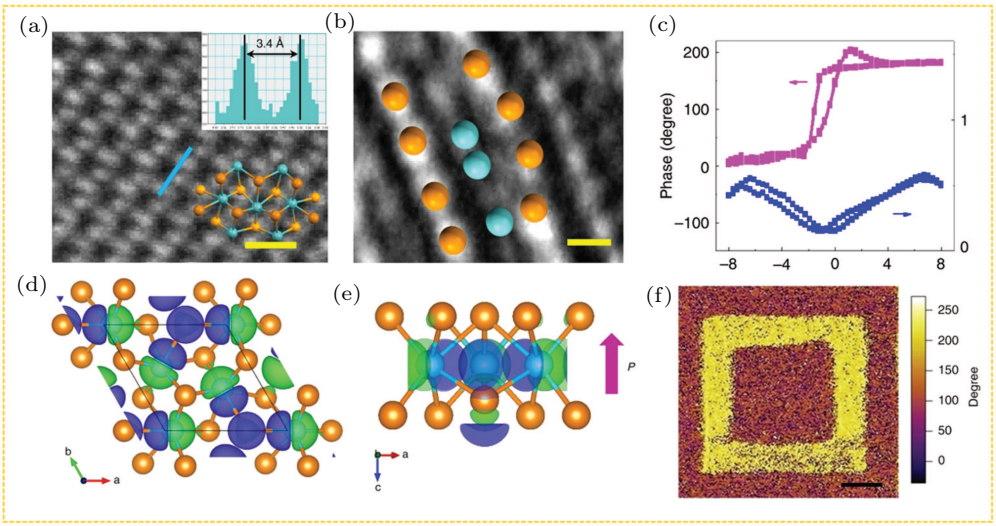


Fig. 6. (a) Top-view high-resolution transmission electron microscopy image and intensity profile of d1T-$MoTe_2$. The scale bar is 0.5 nm. (b) Atomic structure image of monolayer d1T-$MoTe_2$. Cyan and orange represent Mo and Te atoms, respectively, and the scale-bar is 2 Å. (c) Corresponding PFM phase hysteretic and butterfly loops. (d), (e) Top and side views of the charge density difference between ferroelectric d1T and paraelectric 1T phases (green and purple denote negative and positive charge, respectively). (f) PFM phase image of monolayer d1T-$MoTe_2$. The two square patterns were poled with ±8 V and the scale bar is 1 μm. Reproduced with permission from Ref. [58].

2.3. The 2D non-intrinsic ferroelectric materials

2.3.1. Sliding ferroelectricity

In an emerging type of 2D ferroelectric, sliding ferroelectricity can be generated via interlayer nonequivalent stacking of nonferroelectric two-dimensional materials and the polarizations are switchable upon interlayer sliding driven by a vertical electric field.[59] Sliding ferroelectrics enable high-speed data writing with low energy consumption while still ensuring robustness to thermal fluctuations.[60,61]

In 2017, Li and Wu[61] first theoretically predicted sliding ferroelectricity in bilayer BN (Fig. 7(a)) and other 2D bilayer materials (such as AlN, ZnO, MoS_2, GaSe, etc.), in which vertical ferroelectric switching is caused by interlayer translation without involving any vertical ion displacement. In 2020, Xiao *et al.*[62] experimentally revealed an electrically driven interlayer sliding process in WTe_2, which could be applied to design non-volatile memory based on Berry curvature. The corresponding SHG measurements show butterfly curves in both the four-layer and five-layer samples (Fig. 7(c)), suggesting switching between two electrical polarization states. The SHG intensity minimum at the turning point of the four- and five-layer samples shows a significant difference in amplitude, which indicates that 1T′ stacking via interlayer sliding may be involved as an intermediate transition state. Their characteristic lattice excitations were subsequently investigated, and the two phases showed similar Raman frequencies and amplitudes of shear modes, as well as high-frequency vibrations belonging to polar T_d crystal geometries (Fig. 7(b)). Moreover, the corresponding SHG polarization patterns are almost the same with respect to both the pattern types and the lobe orientations (Fig. 7(d)). All these characteristics confirm the occurrence of sliding ferroelectric switching upon electrical stimulation. In 2021, Yasuda *et al.*[63] demonstrated a rational design approach to 2D ferroelectric engineering of nonferroelectric compounds by vdW stacking. In order to investigate the flipping of polarization upon the application of an electric field, (Au/Cr)/hBN/graphene/P-BBN/hBN/(Pd/Au) bipolar vdW heterojunction devices (where P-BBN is parallel stacked bilayer BN) were designed. Additional carriers induced by P-BBN polarization were detected with graphene. Figure 7(e) shows the resistance of the graphene sensor (R_{xx}) as a function of the upper gate voltage (V_T) divided by the thickness of top hBN (d_T), which shows a typical peak value at $V_T/d_T = 0$ without hysteresis. In contrast, Fig. 7(f) shows the presence of hysteresis in the resistance versus the bottom gate voltage (V_B) divided by the distance between graphene and the bottom gate electrode (d_B) for both forward and reverse scans, and this bistability is attributed to polarization switching of the P-BBN in the presence of an applied electric field. The high mobility as well as room-temperature ferroelectricity of graphene paves the way for potential applications in ultrathin non-volatile memories. In 2022, Wan *et al.*[64] demonstrated robust sliding ferroelectricity in semiconducting 1T′-ReS_2 multilayers with vertical polarization at room temperature. The electric polarization can be attributed to the uncompensated charge transfer between layers. In the same year, TMDs were reported to have IP sliding motion or twisting, inducing flipped OOP polarization by stacking two identical monolayer TMDs in parallel.[65,66] In addition to interlayer twisting and interlayer translation, doping was also reported as an effective method to construct the newly emerging sliding ferroelectrics. For instance, yttrium-doped γ-InSe (InSe:Y) shows both OOP and IP ferroelectricity.[67]

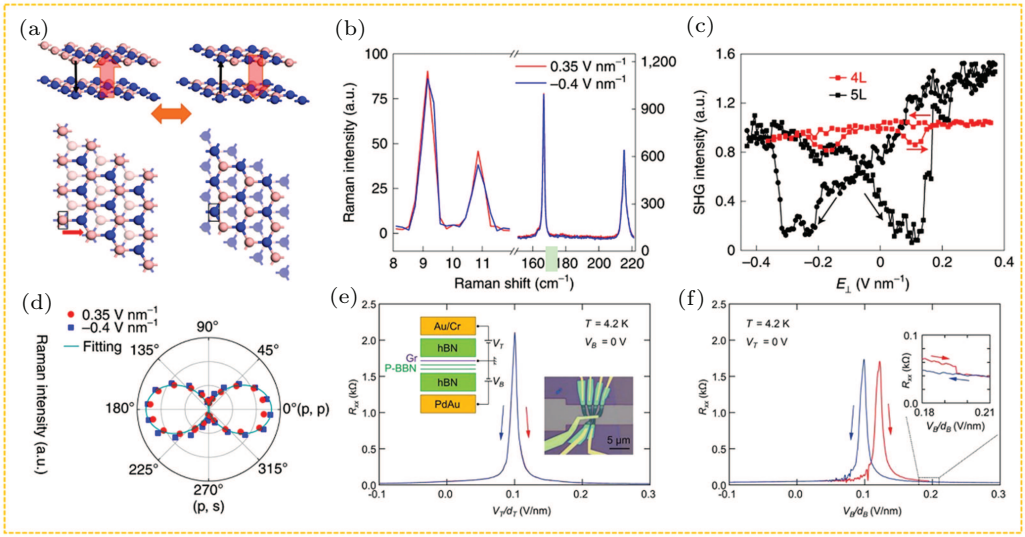


Fig. 7. (a) Ferroelectric switching pathway of a BN bilayer. Pink and blue spheres denote B and N atoms, respectively. (b) Raman spectra of the fully upward and downward poled states in the five-layer T_d-WTe_2 sample. (c) Evolution of *in situ* SHG intensity in the phase transition, driven by a pure E-field sweep on a four-layer (4L) and a five-layer (5L) T_d-WTe_2 device. (d) SHG intensity of fully upward and downward poled phases as a function of analyzer polarization angle. (e), (f) A dual-gated vdW heterostructure device composed of a metal top gate (Au/Cr)/hBN/graphene/0° parallel stacked bilayer BN (P-BBN)/hBN/metal bottom gate (PdAu), and the resistance R_{xx} of graphene as a function of V_T/d_T and V_B/d_B. Reproduced with permission from Refs. [61–63].

Next, the polarization flipping mechanism and cumulative effect in sliding ferroelectrics are analyzed. Polarization reversal is induced by charge transfer between the atomic layers. Meng *et al.*[68] systematically studied the polarization flip kinetics in multilayer 3R-MoS_2. They found that samples have stable and tunable anomalous intermediate polarization states. These anomalous polarization states are related to the antiparallel arrangement of dipoles and strong coupling between the OOP dipoles. Thus, an 'antiparallel polarization model' is proposed for the polarization reversal mechanism (Fig. 8(a)). Taking three-layer 3R-MoS_2 as an example, in the antiparallel polarization model not all atomic layers slide simultaneously while one atomic layer translates or two nonadjacent (adjacent) atomic layers translate (Figs. 8(b)–8(d)). Concerning the cumulative polarization effect, Deb *et al.*[69] investigated the polarization of multilayered TMD stacks, and showed that the polarization is confined to the interlayer interfaces, suggesting that there is weak coupling between adjacent interfaces and hence a cumulative polarization effect in layer stacking. For example, by measuring the potentials at the surface of naturally grown ABC-stacked 3R-MoS_2 crystals it was found that the increase in polarization-aligned layers resulted in a linear increase in total polarization with stack thickness, confirming the cumulative interfacial effect.

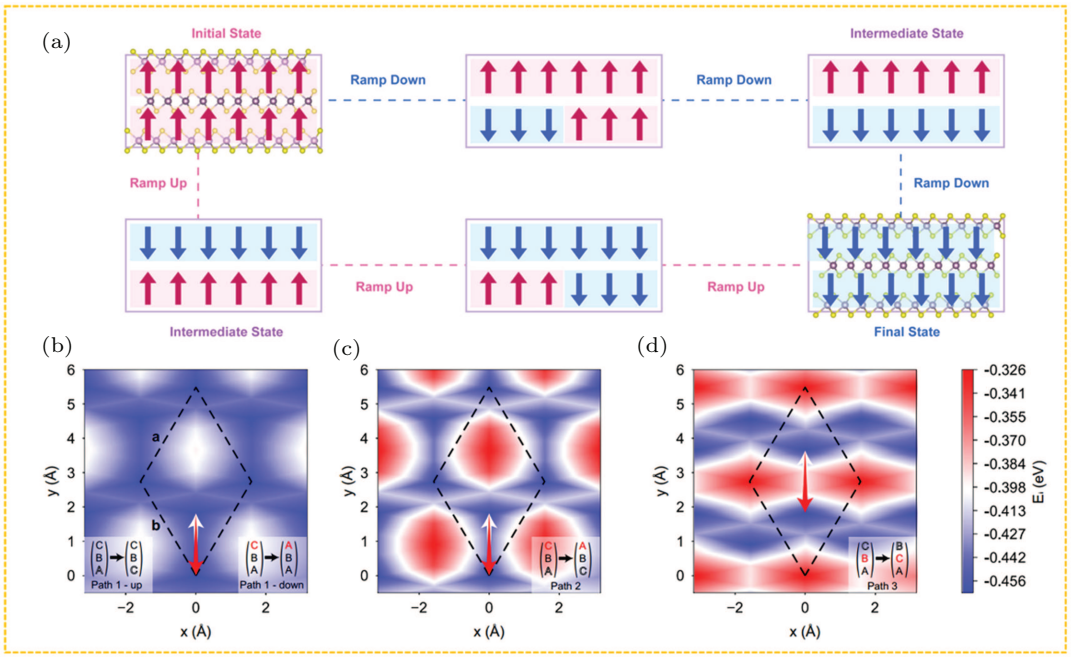


Fig. 8. (a) Schematic of the 'antiparallel polarization model' for three-layer 3R-MoS_2 with an antiparallel arrangement of dipoles. (b)–(d) Potential energy surfaces experienced by the translating atomic layer(s). Reproduced with permission from Ref. [68].

Such unconventional sliding ferroelectrics are of great significance for designing metallic ferroelectrics and solving the issues faced by conventional ferroelectrics. Designing 2D materials with coexisting internal charge dipoles and free electrons is usually challenging as the free charge carriers tend to screen dipole formation and cooperative orientation. The discovery of sliding ferroelectricity suggests a way to overcome the above difficulties by exploiting a partition between IP and OOP phenomena: the IP conductivity is supplied by the mobile 2D carrier gas, whereas the OOP switchable polarization arises from intrinsic symmetry breaking at the interface and interlayer sliding. It is vital to overcome such difficulties for implementing non-volatile memory and rapid logic response in a single material. As is well known, one of the main barriers to the commercialization of conventional ferroelectric-based nanoelectronic devices is their insulation and interface problems, which prevent their integration into semiconductors in nanocircuits and reduce data read/write efficiency. In contrast, interlayer sliding ferroelectrics have many advantages, including facilitating integration into silicon chips, high-speed energy-saving data writing and efficient data reading.[70] These advantages can promote their practical applications.

2.3.2. Moiré ferroelectricity

Moiré ferroelectricity can be induced by a small twist angle in the ferroelectric bilayers, which may enable ultrafast, programmable and atomically thin storage devices. The different ferroelectric domains could be generated by large-scale modulation of local stacking. In 2017, Li and Wu[61] proposed moiré ferroelectricity in a twisted BN bilayer with upward polarization in AB domains and downward polarization in BA domains (Fig. 9(a)). In 2020, Zheng *et al.*[71] observed the emergence of ferroelectricity in graphene-based moiré heterostructures. When the bilayer graphene is sandwiched between two hBN layers, switchable ferroelectricity is achieved by introducing a moiré superlattice lattice potential (Figs. 9(b) and 9(c)). It was observed that the graphene resistance exhibited

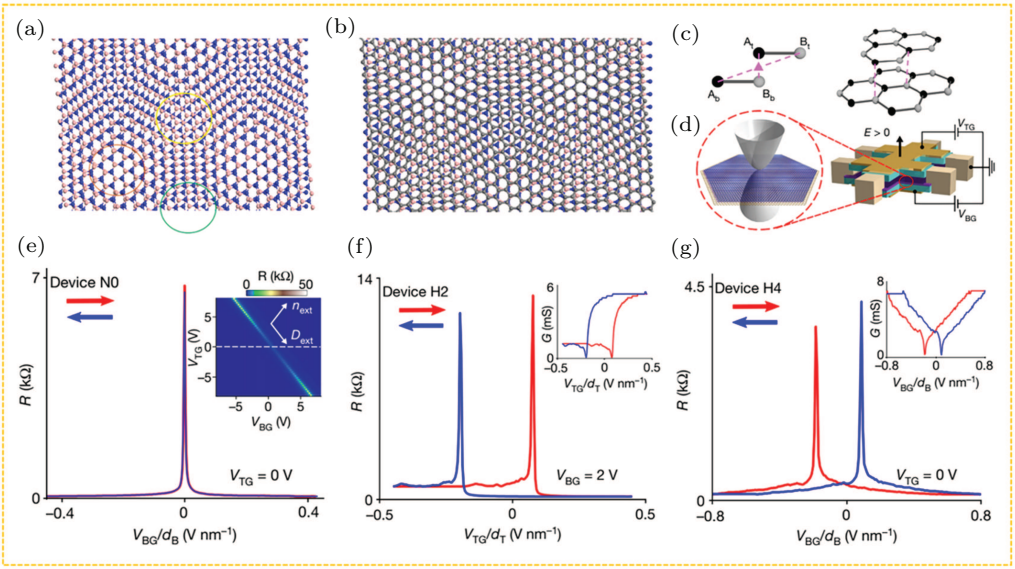


Fig. 9. (a) Lattice structure of Bernal-stacked bilayer graphene. (b) Schematic of the band dispersion and layer polarization of the low-energy electronic states of pristine bilayer graphene at different interlayer electric fields. (c) Schematic of a device with top and bottom gates. (d)–(f) Four-probe resistance for a normal bilayer graphene device N0 and devices H2 and H4. Reproduced with permission from Refs. [61,71].

prominent and robust hysteretic behavior when an externally applied OOP displacement field was applied. Normal bilayer graphene (device N0) shows no hysteresis (Fig. 9(d)), while the resistive hysteresis loops of devices H2 (Fig. 9(e)) and H4 (Fig. 9(f)) have opposite behavior in terms of whether the resistive peaks appear in advance or in retard, indicating the unconventional nature of the ferroelectricity. In 2023, Yang *et al.*[72] predicted atypical moiré ferroelectricity in pure multilayer graphene. Multilayer graphenes with $N > 3$ can all be ferroelectric, which stems from the symmetry breaking by stacking configurations across layers. Polarization can be electrically switched via interlayer sliding.

2.3.3. Defective ferroelectrics

Surface vacancies are unavoidable during the stripping and synthesis process of 2D materials. Although these vacancies usually have negative effects on charge transport, they can enrich the applications of 2D materials in other aspects, such as electric polarization. In 2018, Zhao *et al.*[73] revealed through DFT calculations that in CrI_3 the surface I vacancies would produce switchable OOP polarization without destroying the non-metallic nature. In 2020, He *et al.*[74] showed by first-principles calculations that point defects can effectively break inversion symmetry, resulting in novel ferroelectrics in superlattices composed of otherwise non-ferroelectric $SrTiO_3$

and $SrRuO_3$. In 2021, Xue *et al.*[75] found that in 2D α-Ga_2Se_3 nanoflakes of $\sim$4 nm, switchable polarization was observed at temperatures up to 450 K. This polarization switching was ascribed to the displacement of Ga vacancies between adjacent asymmetric sites through the application of an electric field. As shown in Fig. 10(a), the intrinsic vacancy defect causes polarization in cubic defects of α-Ga_2Se_3. The effect of crystal structure on the SHG intensity was further investigated by polarization-resolved SHG at room temperature (Fig. 10(b)), which exhibits approximate $C6$ symmetry, clearly demonstrating inversion symmetry breaking in the α-Ga_2Se_3 nanosheet. Figures 10(c) and 10(d) show α-Ga_2Se_3 nanoflakes of $\sim$ 4 nm with a high transition temperature of 450 K. Other nanoflake thicknesses (10 nm, 25 nm) also show the same trend of temperature-dependent SHG intensity. This work removes the point group limitation of ferroelectrics and extends the range of 2D ferroelectrics to naturally defective semiconductors.

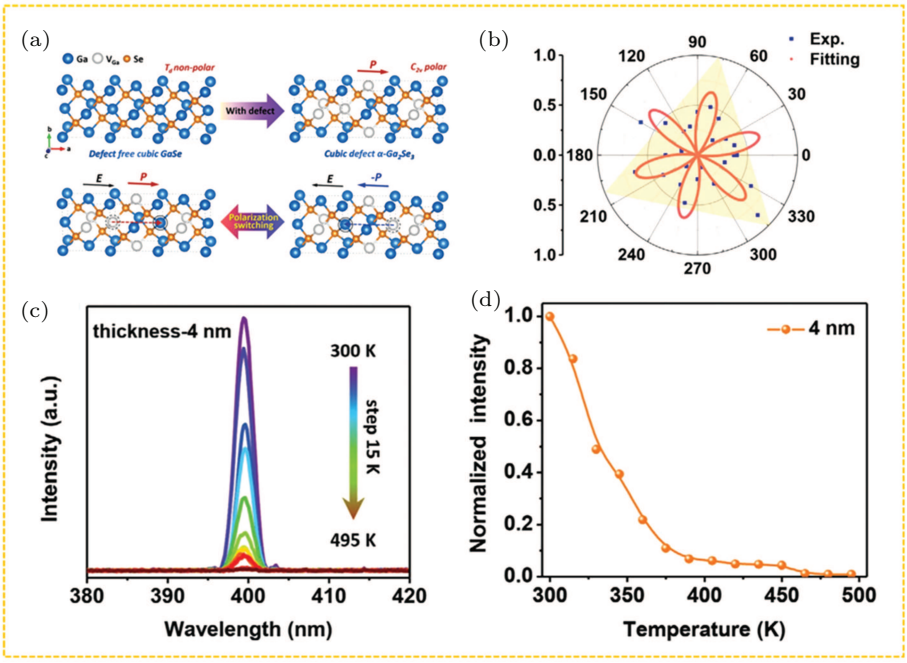


Fig. 10. (a) The polarization induced by native vacancy-defects in defective α-Ga_2Se_3. (b) Polarization angle dependent SHG intensity. (c), (d) Temperature-dependent SHG intensity on 4 nm α-Ga_2Se_3. Reproduced with permission from Ref. [75].

3. Applications of 2D ferroelectric materials

The combination of atom-thick 2D ferroelectrics with low-band-gap high-mobility semiconductors and external field regulation of polarization order enables the 2D ferroelectrics to be applied in various nanodevices, including ferroelectric field-effect transistors, photoelectric storage, computing in memory, efficient ferroelectric photovoltaics and ferroelectric tunnel junctions. Below we summarize these important 2D ferroelectric-based nanodevices.

3.1. Ferroelectric semiconductor field-effect transistors

Ferroelectric field-effect transistors, in which a ferroelectric insulator is used as the gate insulator, can be used for high-density non-volatile memory with fast switching speed on a nanosecond scale. However, they suffer from issues of the depolarization field and the gate leakage current, which causes threshold voltage drift and destruction of the memory states. These issues can be well solved in ferroelectric semiconductor field-effect transistors in which a ferroelectric semiconductor is used as the channel material while the gate insulator is the dielectric (Fig. 11(a)). In 2019, Si *et al.*[76] reported a 2D α-In_2Se_3-based ferroelectric semiconductor field effect transistor with 15-nm-thick HfO_2 as a gate dielectric (Fig. 11(b)). To protect and improve the performance of the transistor, an atomic layer of aluminum oxide (Al_2O_3) was deposited as a passivation layer. Figures 11(c) and 11(d) show the excellent performance of the transistor with a large memory window, a high on/off ratio of $> 10^8$, a maximum on-current of 862 $\mu A \cdot \mu m^{-1}$ and a low supply voltage. These results indicate that ferroelectric semiconductor field-effect transistors have the potential for non-volatile memory.

In addition to the memory application, the vdW ferroelectric semiconductor field-effect transistor shows great potential for in-memory computing. For example, Liao *et al.*[77] constructed an InSe-based metal–oxide–ferroelectric semiconductor field-effect transistor that integrates memory and logic functions in the same ferroelectric material. The OOP ferroelectric polarization in InSe enables data storage and the semiconducting property was adopted for the logic computation; inverter, programmable NAND and NOR Boolean logic operations with non-volatile storage of the results have all been demonstrated nicely.

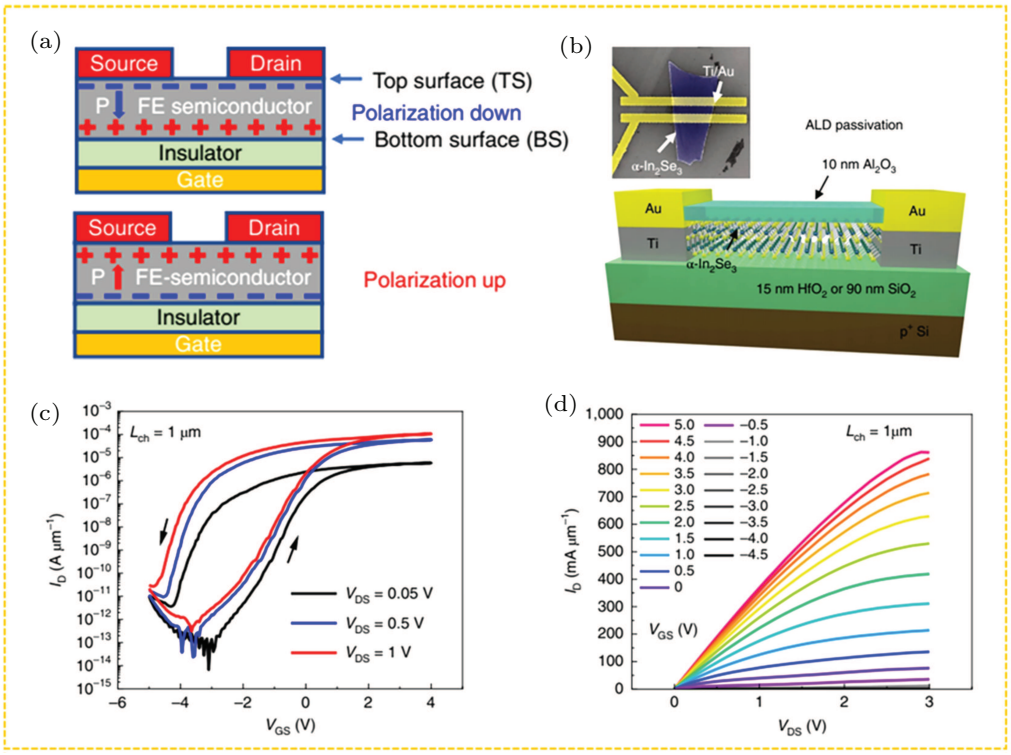


Fig. 11. (a) Schematic diagram of a ferroelectric semiconductor field-effect transistor with polarization charge distributions corresponding to polarization down and polarization up states. (b) Structure diagram of an α-In_2Se_3 ferroelectric semiconductor field-effect transistor with a HfO_2 gate insulator and Al_2O_3 passivation layer. (c) I_D–V_{GS} and (d) I_D–V_{DS} of the transistor. Reproduced with permission from Ref. [76].

3.2. Photoelectric storage

Photo-controlled ferroelectric domains have potential applications in the field of optoelectronic storage and have become an interesting and important topic in modern solid-state physics. However, conventional ferroelectrics usually face huge challenges such as poor conductivity and mismatch between incident photons and ferroelectric switching energy. The 2D ferroelectric semiconductor materials have great potential for optoelectronic memories based on a light-modulated polarization reversal capability. In 2020, Xue *et al.*[78] demonstrated optoelectronic memory applications of a 2D α-In_2Se_3 ferroelectric semiconductor through optical and electrical engineering of the ferroelectric domain wall in a non-volatile manner. The memory has a high on/off ratio of over 10^4 using optical writing and electrical erasure. Non-volatile photoresponses are shown in Fig. 12(a). The green area indicates the current response under white light and the yellow area indicates the non-volatile current obtained by applying a +0.3 V read voltage after removing the white light. In the initial state, the light-induced current switching ratio is 81, after +4 V polarization the switching ratio is only 2.5, and after −4 V polarization the switching ratio reaches 1.6×10^4. Figure 12(b) shows highly reproducible optical writing and electrical erasing processes. The current values in the pink area indicate the 'off' state, while the current values in the yellow area indicate the non-volatile 'on' state. The device used in this work has a simple structure, a high write–erase current ratio ($> 10^4$), an off-state current below 10^{-13} A and broad-spectrum optical information storage. In 2022, Lv *et al.*[79] constructed an α-In_2Se_3-based multilevel memory by modulating the polar order by applying an in-plane electric field. Three switchable resistive states were achieved with a fast switching speed, good endurance and retention. Notably, reversible switching between the intermediate- and low-resistance states can be achieved by an ultra-low electric field one to two orders of magnitude smaller than that of other memories based on 2D ferroelectric materials. Furthermore, it is found that these three different polar-order states exhibit a characteristic optical response. These reports indicate that the 2D ferroelectric semiconductor materials have great potential for non-volatile high-density optoelectronic memories.

By taking advantage of the ferroelectric, optoelectronic and semiconducting properties offered by α-In_2Se_3, Liu *et al.*[80] constructed an optoelectronic synapse based on α-In_2Se_3. As a result of the tight coupling between ferroelectric and optoelectronic processes in the synapse, heterosynaptic plasticity with controllable temporal dynamics under electrical and optical stimuli has been realized. These properties provide a basis for creating a multimode and multiscale reservoir computing system with adjustable nonlinear transformation and multisensory fusion, which could be utilized to accomplish complex tasks such as multimode handwritten digit recognition, QR code recognition and temporal signal prediction.

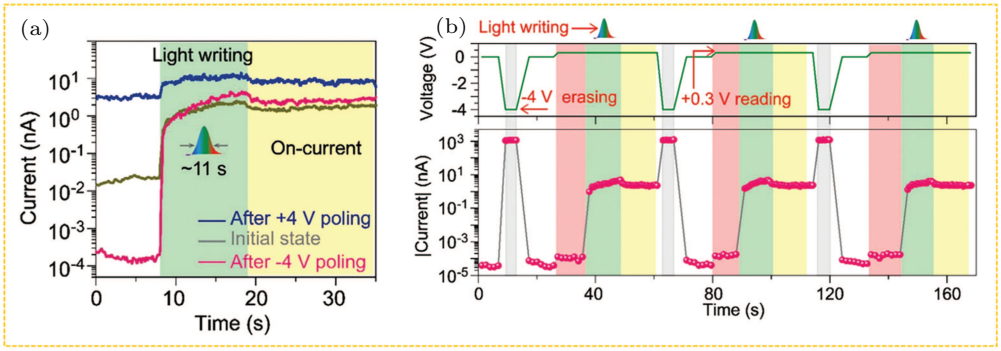


Fig. 12. (a) Non-volatile photoresponses of a 2D α-In_2Se_3 ferroelectric semiconductor in different conditions including the initial state and after -4 V poling and $+4$ V poling. (b) Dynamic current responses with alternating optical writing and electrical erasure. Reproduced with permission from Ref. [78].

3.3. Synaptic simulations

Synaptic simulation devices are crucial for the implementation of hardware-based artificial neuromorphic devices and for the construction of high-density efficient emerging memory computing integrators. The external field regulation of polarization-order 2D ferroelectrics can be used for synaptic simulations. In 2020, Kwon *et al.*[81] reported in-plane synaptic simulation in a metal/ferroelectric semiconductor/metal (Pt/SnS ($<$ 6 nm)/Pt) device (Fig. 13(a)). The electronic synapse device exhibited highly stable room-temperature operation, high linearity of potentiation/depression, long retention and low variation. Figure 13(b) shows the transition from short-term plasticity to long-term plasticity (LTP) by increasing the pulse amplitude. A large ratio between maximum conductance and minimum conductance (G_{max}/G_{min}) and linear LTP/LTD curves was obtained by applying incremental voltage spikes (Fig. 13(c)), which gives rise to high accuracy in pattern recognition in artificial neural network simulations.

By using the vdW semiconducting ferroelectric α-In_2Se_3 with interlocked IP and OOP polarization, Xue *et al.*[82] found that ferroelectric polarization of the α-In_2Se_3 nanoflakes can be toggled by an electric field along any direction, enabling a memristor with distinct switching characteristics where the read current can be modulated by applying electrical pulses at various terminal pairs. Moreover, the third terminal of the memristor exhibits non-volatile control over channel current at a pico-Ampere level, endowing the device with low operational energy consumption (pico-Joule read energy), excellent endurance (1000 cycles) and long-term retention (57 h). Furthermore, multiterminal memristors exhibit typical heterosynaptic plasticity with a resistance–switching ratio of above 10^3, which holds great potential for applications in brain-inspired computing systems and logic-in-memory computers.

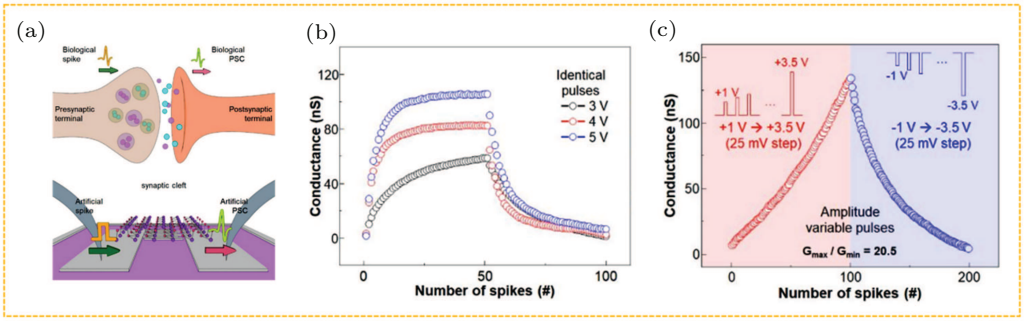


Fig. 13. (a) Schematic illustration comparing biological and artificial synapses. (b) Postsynaptic current changes as a function of the number of spikes with different pulse amplitudes (from $\pm$3 V to $\pm$5 V). (c) Conductance changes in potentiation and depression of the fabricated device with an incremental pulse scheme. Reproduced with permission from Ref. [81].

3.4. Bulk photovoltaic effect

The bulk photovoltaic effect (BPVE) has been a focus of research in the photovoltaic field in recent years.[83–85] It mainly refers to the phenomenon whereby spontaneous photocurrent only occurs in crystals with broken inversion symmetry under illumination and does not require a p–n junction. The BPVE is expected to break the theoretical limit for photoelectric conversion efficiency of p–n junctions and achieve a photogenerated voltage that exceeds the material band gap.[86] Ferroelectrics are typical polar crystals and can generate BPVE. Compared with the three-dimensional ferroelectrics dominated by perovskite oxides (such as $BiFeO_3$, $PbTiO_3$, etc.), higher photocurrent densities can be obtained through the high electron state density and the shift current related to the band Berry phase in low-dimensional material systems.[87] Furthermore, polarization regulation of 2D ferroelectric materials has been proven to be a feasible way to effectively optimize photovoltaic performance. For example,

in recent work a vertical heterostructure was constructed using graphene with a few layers of $CuInP_2S_6$, and the electric polarization state was modulated by an external electric field, thereby enhancing or suppressing the photocurrent, as shown in Figs. 14(a) and 14(b).[87] Strain-induced ferroelectric polarization can also significantly enhance the BPVE of noncentrosymmetric 3R-MoS_2 multilayers. When an IP tensile strain of $\sim 0.2\%$ was applied, the photocurrent increased by more than two orders of magnitude (Figs. 14(c) and 14(d)).[88] In addition, the results of first-principles calculations for interlayer sliding ferroelectrics show that the IP BPVE coefficient is invariant with change in the ferroelectric order, while the OOP BPVE coefficient is reversed with switching of ferroelectric order. These results can provide guidance for constructing photoelectric devices by using the relationship between BPVE and ferroelectric order.[89] For example, it is possible to construct larger-scale photoelectric devices by utilizing the insensitive properties of the IP BPVE, and to design switchable photoelectric devices by utilizing the OOP BPVE. Theoretical calculations have also predicted BPVE of SnTe monolayers,[90] MX $[M = (\mathrm{Ge}, \mathrm{Sn}), X = (\mathrm{Se}, \mathrm{S})]$[91] and WTe_2.[92]

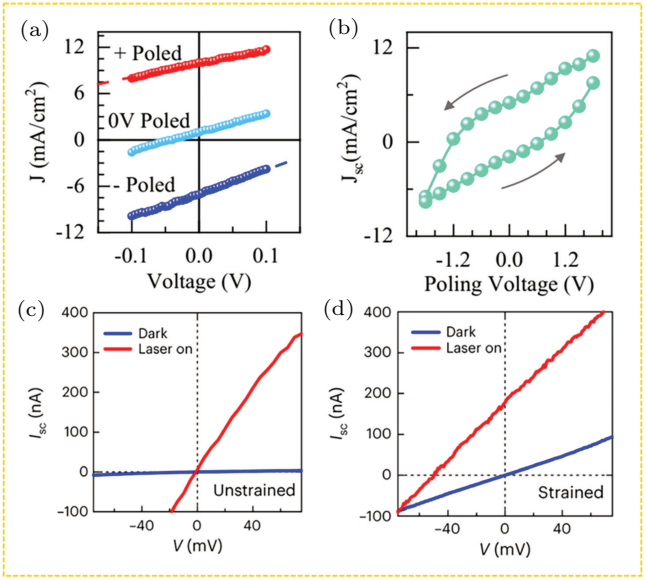


Fig. 14. (a) Extracted output I–V curves at specific poling voltages. (b) The plot of J_{sc} as a function of the poling voltage. (c), (d) The I–V characteristics of an unstrained 3R-MoS_2 device (c) and a strained ($\sim 0.18\%$) 3R-MoS_2 device (d). Reproduced with permission from Refs. [87,88].

3.5. Ferroelectric tunnel junctions

A ferroelectric tunnel junction (FTJ) is composed of two metal electrodes separated by an ultrathin ferroelectric as the barrier. By adjusting the polarization of the ferroelectric layer in an FTJ, non-volatile switching between high (off-state) and low (on-state) tunneling resistance (TER) can be realized.[93,94] The exploration of ways to improve tunneling electroresistance is a long-term pursuit.[95] Because of their advantages of non-destructive readout, high storage density, ultra-fast data access and low energy consumption, FTJs have been studied experimentally based on 2D ferroelectrics. For example, $CuInP_2S_6$ has been used as the ferroelectric barrier, and graphene and chromium as asymmetric contacts to construct an FTJ. A barrier height modulation of 1 eV can be caused in the junction, which results in a TER of over 10^7.[96] Recently, a giant TER of $\sim 10^4\%$ was also achieved in a vdW sliding FTJ with the sliding ferroelectric bilayer hBN as an ultrathin barrier. This exciting result implies that layer-engineered 2D vdW sliding ferroelectrics have potential applications in ferroelectric memory devices.[97] In addition to the aforementioned FTJ, a two-dimensional antiferroelectric tunnel junction was also demonstrated.[98]

4. Summary and outlook

Ferroelectric materials have stable and switchable spontaneous polarization that can be controlled by external electric fields and are used in a wide range of applications. This review article focuses on the progress of experimental research into 2D ferroelectric materials, where stable spontaneous polarization has been found in materials with a few atomic layers. The limitations of size effects in conventional ferroelectric materials are broken based on observed ferroelectricity in single-atomic-layer films. The IP and OOP interlocked ferroelectricity at room temperature is potentially advantageous in many electronic applications. The discovery of pure IP ferroelectricity solves the problem of the depolarization field at the metal–ferroelectric interface. The unique structural and electrical properties of 2D ferroelectric materials open up possibilities for many new device applications, including non-volatile memories, logic-in-memory computers and energy harvesters.

The 2D ferroelectric materials are a cutting-edge research topic, they exhibit excellent mechanical, thermal, optical and electrical properties, which form a basis for disruptive innovations in many fields. Despite the various unique advantages offered by 2D ferroelectric materials, their exploration is still at an early stage and challenges must be overcome for practical application.

(1) From the materials aspect, it is crucial to discover more sliding ferroelectrics by expanding them from binary compounds to mono-element systems and ternary compounds. Furthermore, new 2D ferroelectric contenders with larger polarization and strategies for enhancing the polarization need to be explored. In addition, the fabrication of large-area (especially wafer-scale) 2D ferroelectric films with controllable thicknesses is highly desirable for practical applications.

(2) From the device aspect, to prepare devices with monolayer ferroelectrics and to explore their optical–electrical properties is of utmost importance; this could pave the way for constructing ultra-high-density information devices. Moreover, constructing devices with more functionalities (such as

the integration of sensing–memory–computing), especially at the wafer scale, needs to be pursued in the future.

(3) From the application aspect, integration of 2D ferroelectric functional devices on silicon needs to be fulfilled to accelerate their practical applications. In the future, we also need to correlate more 2D materials with practical applications by designing new 2D multiferroics for high-capacity storage devices.

Acknowledgements

Project supported by the National Key Research and Development Program of China (Grant No. 2022YFB3505301), the National Natural Science Foundation of China (Grant Nos. 12241403 and12174237), and the Graduate Education Innovation Project in Shanxi Province (Grant No. 2021Y484).

References

[1] Valasek J 1921 *Phys. Rev.* **17** 475
[2] Busch G and Scherrer P 1935 *Naturwissenschaften* **23** 737
[3] Von Hippel A 1950 *Rev. Mod. Phys.* **22** 221
[4] Furukawa T 1984 *Ferroelectrics* **57** 63
[5] Yagi T, Tatemoto M and Sako J I 1980 *Polym. J.* **12** 209
[6] Bune A V, Fridkin V M, Ducharme S, Blinov L M, Palto S P, Sorokin A V, Yudin S G and Zlatkin A 1998 *Nature* **391** 874
[7] Ji D X, Cai S H, Paudel T R, Sun H Y, Zhang C C, Han L, Wei Y F, Zang Y P, Gu M and Zhang Y 2019 *Nature* **570** 87
[8] Cheema S S, Kwon D, Shanker N, Reis Rd, Hsu S L, Xiao J, Zhang H G, Wagner R, Datar A and McCarter M R 2020 *Nature* **580** 478
[9] Novoselov K S, Geim A K, Morozov S V, Jiang D, Zhang Y, Dubonos S V, Grigorieva I V and Firsov A A 2004 *Science* **306** 666
[10] Chhowalla M, Shin H S, Eda G, Li L J, Loh K P and Zhang H 2013 *Nat. Chem.* **5** 263
[11] Huang X, Zeng Z and Zhang H 2013 *Chem. Soc. Rev.* **42** 1934
[12] Chhowalla M, Liu Z and Zhang H 2015 *Chem. Soc. Rev.* **44** 2584
[13] Wang Q H, Kalantar-Zadeh K, Kis A, Coleman J N and Strano M S 2012 *Nat. Nanotechnol.* **7** 699
[14] Lin Y, Williams T V and Connell J W 2010 *J. Phys. Chem. Lett.* **1** 277
[15] Anasori B, Lukatskaya M R and Gogotsi Y 2017 *Nat. Rev.* **2** 16098
[16] Naguib M, Mochalin V N, Barsoum M W and Gogotsi Y 2014 *Adv. Mater.* **26** 992
[17] Chandrasekaran A, Mishra A and Singh A K 2017 *Nano Lett.* **17** 3290
[18] Houssa M, Scalise E, Sankaran K, Pourtois G, Afanas'ev V V and Stesmans A 2011 *Appl. Phys. Lett.* **98** 223107
[19] Senger R T, Tongay S, Durgun E and Ciraci S 2005 *Phys. Rev. B* **72** 075419
[20] Lalmi B, Oughaddou H, Enriquez H, Kara A, Vizzini S, Ealet B and Aufray B 2010 *Appl. Phys. Lett.* **97** 223109
[21] Liu H, Du Y C, Deng Y X and Ye P D 2015 *Chem. Soc. Rev.* **44** 2732
[22] Kara A, Enriquez H, Seitsonen A P, Lew Yan Voon L C, Vizzini S, Aufray B and Oughaddou H 2012 *Surf. Sci. Rep.* **67** 1
[23] Bianco E, Butler S, Jiang S S, Restrepo O D, Windl W and Goldberger J E 2013 *ACS Nano* **7** 4414
[24] Peng Y, Li Y S, Ban Y J, Jin H, Jiao W M, Liu X L and Yang W S 2014 *Science* **346** 1356
[25] Rodenas T, Luz I, Prieto G, Seoane B, Miro H, Corma A, Kapteijn F, Xamena F X L I and Gascon J 2015 *Nat. Mater.* **14** 48
[26] Colson J W, Woll A R, Mukherjee A, Levendorf M P, Spitler E L, Shields V B, Spencer M G, Park J and Dichtel W R 2011 *Science* **332** 228
[27] Kory M J, Wörle M, Weber T, Payamyar P, Poll Stan W van de, Dshemuchadse J, Trapp N and Schlüter A D 2014 *Nat. Chem.* **6** 779
[28] Kissel P, Murray D J, Wulftange W J, Catalano V J and King B T 2014 *Nat. Chem.* **6** 774
[29] Wu J B, Chen H Y, Yang N, Cao J, Yan X D, Liu F X, Sun Q B, Ling X, Guo J and Wang H 2020 *Nat. Electron.* **3** 466
[30] Liu F C, You L, Seyler K L, Li X B, Yu P, Lin J H, Wang X W, Zhou J D, Wang H and He H Y 2016 *Nat. Commun.* **7** 12357
[31] Wan S Y, Li Y, Li W, Mao X Y, Zhu W G and Zeng H L 2018 *Nanoscale* **10** 14885
[32] Wang X W, Yu P, Lei Z D, Zhu C, Cao X, Liu F C, You L, Zeng Q S, Deng Y and Zhu C 2019 *Nat. Commun.* **10** 3037
[33] Si M W, Saha A K, Gao S J, Qiu G, Qin J K, Duan Y Q, Jian J, Niu C, Wang H Y and Wu W Z 2019 *Nat. Electron.* **2** 580
[34] Xue F, He X, Liu W H, Periyanagounder D, Zhang C H, Chen M G, Lin C H, Luo L Q, Yengel E and Tung V 2020 *Adv. Funct. Mater.* **30** 2004206
[35] Xue W H, Gao C H, Zhang Z, Han T T, Hou N, Yin W H, Shi L, Wang X L, Liu G, Xu X H 2023 *Sci. China Mater.* **66** 764
[36] Belianinov A, He Q, Dziaugys A, Maksymovych P, Eliseev E, Borisevich A, Morozovska A, Banys J, Vysochanskii Y and Kalinin S V 2015 *Nano Lett.* **15** 3808
[37] Susner M A, Belianinov A, Borisevich A, He Q, Chyasnavichyus M, Demir H, Sholl D S, Ganesh P, Abernathy D L, McGuire M A and Maksymovych P 2015 *ACS Nano* **9** 12365
[38] Huang Y T, Chen N K, Li Z Z, Wang X P, Sun H B, Zhang S B and Li X B 2022 *InfoMat.* **4** e12341
[39] Abrahams S C 1990 *Ferroelectrics* **104** 37
[40] Ding W J, Zhu J B, Wang Z, Gao Y F, Xiao D, Gu Y, Zhang Z Y and Zhu W G 2017 *Nat. Commun.* **8** 14956
[41] Cui C J, Hu W J, Yan X X, Addiego C, Gao W P, Wang Y, Wang Z, Li L Z, Cheng Y C and Li P 2018 *Nano Lett.* **18** 1253
[42] Poh S M, Tan S J R, Wang H, Song P, Abidi I H, Zhao X X, Dan J D, Chen J S, Luo Z T and Pennycook S J 2018 *Nano Lett.* **18** 6340
[43] Xue F, Hu W J, Lee K C, Lu L S, Zhang J W, Tang H L, Han A, Hsu W T, Tu S B and Chang W H 2018 *Adv. Funct. Mater.* **28** 1803738
[44] Io W F, Yuan S G, Pang S Y, Wong L W, Zhao J and Hao J H T 2020 *Nano Res.* **13** 1897
[45] Lv B H, Yan Z, Xue W H, Yang R L, Li J Y, Ci W J, Pang R X, Zhou P, Liu G and Liu Z Y 2021 *Mater. Horiz.* **8** 1472
[46] Lv B H, Xue W H, Yan Z, Yang R L, Wu H, Wang P, Zhang Y Y, Hou J N, Zhu W G and Xu X H 2022 *Sci. China Mater.* **65** 1639
[47] Hu H, Sun Y, Chai M, Xie D, Ma J and Zhu H 2019 *Appl. Phys. Lett.* **114** 252903
[48] Hu H, Wang H, Sun Y, Li J, Wei J, Xie D and Zhu H 2021 *Nanotechnology* **32** 385202
[49] Wu M H and Zeng X C 2016 *Nano Lett.* **16** 3236
[50] Higashitarumizu N, Kawamoto H, Lee C J, Lin B H, Chu F H, Yonemori I, Nishimura T, Wakabayashi K, Chang W H and Nagashio K 2020 *Nat. Commun.* **11** 2428
[51] Anderson P P W and Blount E I 1965 *Phys. Rev. Let.* **14** 217
[52] Shi Y G, Guo Y F, Wang X, Princep A J, Khalyavin D, Manuel P, Michiue Y, Sato A, Tsuda K and Yu S 2013 *Nat. Mater.* **12** 1024
[53] Fei Z Y, Zhao W J, Palomaki T A, Sun B S, Miller M K, Zhao Z Y, Yan J Q, Xu X D and Cobden D H 2018 *Nature* **560** 336
[54] Sharma P, Xiang F X, Shao D F, Zhang D, Tsymbal E Y, Hamilton A R and Seidel J 2019 *Sci. Adv.* **5** eaax5080
[55] Ma X Y, Lyu H Y, Hao K R, Zhao Y M, Qian X F, Yan Q B and Su G 2021 *Sci. Bull.* **66** 233
[56] Qi L, Ruan S C and Zeng Y J 2021 *Adv. Mater.* **33** 2005098
[57] Xiao C C, Xu Z A, Luo X and Lu Y H 2001 arXiv 03164 [cond-mat.mes-hall]
[58] Yuan S G, Luo X, Chan H L, Xiao C C, Dai Y W, Xie M H and Hao J H 2019 *Nat. Commun.* **10** 1775
[59] Wu M H and Li J 2021 *P. Natl. Acad. Sci. USA* **118** e211570311
[60] Wu M H 2021 *ACS Nano* **15** 9229
[61] Li L and Wu M H 2017 *ACS Nano* **11** 6382
[62] Xiao J, Wang Y, Wang H, Pemmaraju C D, Wang S Q, Muscher P, Sie E J, Nyby C M and Devereaux T P 2020 *Nat. Phys.* **16** 1028
[63] Yasuda K J, Wang X R, Watanabe K J, Taniguchi T and Jarillo-Herrero P 2021 *Science* **372** 1458
[64] Wan Y, *et al.* 2022 *Phys. Rev. Lett.* **128** 067601
[65] Wang X, Yasuda K, Zhang Y, Liu S, Watanabe K, Taniguchi T, Hone J and Fu L, Jarillo-Herrero P 2022 *Nat. Nanotechnol.* **17** 367
[66] Weston A, *et al.* 2022 *Nat. Nanotechnol.* **17** 390
[67] Sui F, Jin M, Zhang Y, Qi R, Wu Y N, Huang R, Yue F and Chu J 2023 *Nat. Commun.* **14** 36
[68] Meng P, Wu Y, Bian R, Pan E, Dong B, Zhao X X, Chen J G, Wu L S, Sun Y Q and Fu Q D 2022 *Nat. Commun.* **13** 7696

[69] Deb S, Cao W, Raab N, Watanabe K J, Taniguchi T, Goldstein M, Kronik L, Urbakh M, Hod O and Shalom M B 2022 *Nature* **612** 465

[70] Vizner Stern M, Waschitz Y, Cao W, Nevo I, Watanabe K, Taniguchi T, Sela E, Urbakh M, Hod O and Ben Shalom M 2021 *Science* **372** 1462

[71] Zheng Z, Ma Q, Bi Z, *et al.* 2020 *Nature* **588** 71

[72] Yang L, Ding S P, Gao J H and Wu M H 2023 *Phys. Rev. Lett.* **131** 096801

[73] Zhao Y H, Lin L F, Zhou Q H, Li Y H, Yuan S J, Chen Q, Dong S and Wang J L 2018 *Nano Lett.* **18** 2943

[74] He R, Lin J L, Liu Q, Liao Z L, Shui L L, Wang Z J, Zhong Z C and Li R W 2020 *ACS Appl. Mater. Interfaces* **12** 45602

[75] Xue W H, Jiang Q T, Wang F K, He R, Pang R X, Yang L, Wang P, Yang R L, Zhong Z C and Zhai T Y 2022 *Small* **18** 2105599

[76] Si M W, Saha A K, Gao S J, Qiu G, Qin J K, Duan Y Q, Jian J, Niu C, Wang H Y and Wu W Z 2019 *Nat. Electron.* **2** 580

[77] Liao J, Wen W, Wu J, Zhou Y, Hussain S, Hu H, Li J, Liaqat A, Zhu H, Jiao L, Zheng Q and Xie L 2023 *ACS Nano* **17** 6095

[78] Xue F, He X, Liu W H, Periyanagounder D, Zhang C H, Chen M G, Lin C H, Luo L Q, Yengel E and Tung V 2020 *Adv. Funct. Mater.* **30** 2004206

[79] Lv B H, Xue W H, Yan Z, Yang R L, Wu H, Wang P, Zhang Y Y, Hou J N, Xu X H and Zhu W G 2022 *Sci. China Mater.* **65** 1639

[80] Liu K, Zhang T, Dang B, *et al.* 2022 *Nat. Electron.* **5** 761

[81] Kwon K C, Zhang Y S, Wang L, Yu W, Wang X J, Park I H, Choi H S, Ma T, Zhu Z Y and Tian B B 2020 *ACS Nano* **14** 7628

[82] Fei Xue, Xin He, Zhenyu Wang, *et al.* 2021 *Adv. Mater.* **33** 2008709

[83] Zhang Y J, Ideue T, Onga M, Qin F, Suzuki R, Zak A, Tenne R, Smet J H and Iwasa Y 2019 *Nature* **570** 349

[84] Akamatsu T, Ideue T, Zhou L, Dong Y, Kitamura S, Yoshii M, Yang D, Onga M, Nakagawa Y and Watanabe K 2021 *Science* **372** 68

[85] Jiang J, Chen Z, Hu Y, Xiang Y, Zhang L, Wang Y, Wang G C and Shi J 2021 *Nat. Nanotechnol.* **16** 894

[86] Spanier J E, Fridkin V M, Rappe A M, Akbashev A R, Polemi A, Qi Y B, Gu Z Q, Young S M, Hawley C J and Imbrenda D 2016 *Nat. Photonics* **10** 611

[87] Li Y, Fu J, Mao X, Chen C, Liu H, Gong M, Zeng H 2021 *Nat. Commun.* **12** 5896

[88] Dong Y, Yang M M, Yoshii M, Matsuoka S, Kitamura S, Hasegawa T, Ogawa N, Morimoto T, Ideue T and Iwasa Y 2023 *Nat. Nanotechnol.* **18** 36

[89] Xiao R C, Gao Y, Jiang H, Gan W, Zhang C and Li H 2022 *npj Comput. Mater.* **8** 138

[90] Kim J, Kim K W, Shin D, Lee S H, Sinova J, Park N and Jin H 2019 *Nat. Commun.* **10** 3965

[91] Wang H and Qian X 2019 *Sci. Adv.* **5** eaav9743

[92] Wang H and Qian X 2019 *npj Comput. Mater.* **5** 119

[93] Pantel D, Goetze S, Hesse D and Alexe M 2012 *Nat. Mater.* **11** 289

[94] Garcia V, Bibes M, Bocher L, Valencia S, Kronast F, Crassous A, Moya X, Enouz-vedrenne S, Gloter A and Imhof D 2010 *Science* **327** 1106

[95] Wen Z, Li C, Wu D, Li A D and Ming N B 2013 *Nat. Mater.* **12** 617

[96] Wu J B, Chen H Y, Yang N, Cao J, Yan X D, Liu F X, Sun Q B, Ling X, Guo J and Wang H 2020 *Nat. Electron.* **3** 466

[97] Yang J, Zhou J, Lu J, Luo Z C, Yang J B and Shen L 2022 *Mater. Horiz.* **9** 1422

[98] Ding J, Shao D F, Li M, Wen L W and Tsymbal E Y 2021 *Phys. Rev. Lett.* **126** 057601